

# Neural-Pull: Learning Signed Distance Functions from Point Clouds by Learning to Pull Space onto Surfaces

Baorui Ma\*

School of Software, BNRist, Tsinghua University  
Beijing, P. R. China

mbr18@mails.tsinghua.edu.cn

Yu-Shen Liu<sup>†</sup>

School of Software, BNRist, Tsinghua University  
Beijing, P. R. China

liuyushen@tsinghua.edu.cn

Zhizhong Han\*

University of Maryland, College Park  
College Park, MD, USA

h312h@umd.edu

Matthias Zwicker

University of Maryland, College Park  
College Park, MD, USA

zwicker@cs.umd.edu

## Abstract

*Reconstructing continuous surfaces from 3D point clouds is a fundamental operation in 3D geometry processing. Several recent state-of-the-art methods address this problem using neural networks to learn signed distance functions (SDFs). In this paper, we introduce Neural-Pull, a new approach that is simple and leads to high quality SDFs. Specifically, we train a neural network to pull query 3D locations to their closest neighbors on the surface using the predicted signed distance values and the gradient at the query locations, both of which are computed by the network itself. The pulling operation moves each query location with a stride given by the distance predicted by the network. Based on the sign of the distance, this may move the query location along or against the direction of the gradient of the SDF. This is a differentiable operation that allows us to update the signed distance value and the gradient simultaneously during training. Our outperforming results under widely used benchmarks demonstrate that we can learn SDFs more accurately and flexibly for surface reconstruction and single image reconstruction than the state-of-the-art methods.*

## 1. Introduction

Signed Distance Functions (SDFs) have been an important 3D shape representation for deep learning based 3D shape analysis [51, 54, 55], due to their advantages over other representations in representing high resolution shapes with arbitrary topology. Given ground truth signed distance

values, it is intuitive to learn an SDF by training a deep neural network to regress signed distance values for query 3D locations, where an image [51, 54] or a point cloud [35, 12] representing the shape can serve as a condition which is an additional input of the network. It has also been shown how to learn SDFs from multiple 2D images rather than 3D information using differentiable renderers [45, 37, 68, 67]. In this paper, we address the problem of learning SDFs from raw point clouds and propose a new method that outperforms the current state of the art on widely used benchmarks.

Current solutions [16, 10, 1, 2] aim to estimate unsigned distance fields by leveraging additional constraints. The rationale behind these solutions is that an unsigned distance field can be directly learned from the distances between a set of query 3D locations and their nearest neighbors on the 3D point clouds, while the signs of these distances require more information to infer, such as geometric regularization [16], sign agnostic learning [1, 2], or analytical gradients [10].

In this paper, we propose a method to learn SDFs directly from raw point clouds without requiring ground truth signed distance values. Our method learns the SDF from a point cloud, or from multiple point clouds with conditions by training a neural network to learn to pull the surrounding 3D space onto the surface represented by the point cloud. Hence we call our method *Neural-Pull*. Specifically, given a 3D query location as input to the network, we ask the network to pull it to its closest point on the surface using the predicted signed distance value and the gradient at the query location, both of which are calculated by the network itself. The pulling operation is differentiable, and depending on the sign of the predicted distance, it moves the query

\*Equal contribution

<sup>†</sup>Corresponding author

location along or against the direction of the gradient with a stride given by the signed distance. Since our training objective involves both the signed distance and its gradient, it leads to highly effective learning. Our experiments using widely used benchmarks show that Neural-Pull can learn SDFs more accurately and flexibly when representing 3D shapes in different applications than previous state-of-the-art methods. Our contributions are listed below.

- i) We introduce Neural-Pull, a novel approach to learn SDFs directly from raw 3D point clouds without ground truth signed distance values.
- ii) We introduce the idea to effectively learn SDFs by updating the predicted signed distance values and the gradient simultaneously in order to pull surrounding 3D space onto the surface.
- iii) We significantly improve the state-of-the-art accuracy in surface reconstruction and single image reconstruction under various benchmarks.

## 2. Related Work

Deep learning models have been playing an important role in different 3D computer vision applications [54, 49, 52, 65, 27, 17, 60, 4, 58, 28, 3, 50, 18, 23, 21, 24, 25, 29, 30, 20, 32, 26, 22, 47, 46, 31, 34, 33, 19, 64]. In the following, we will briefly review work related to learning implicit functions for 3D shapes in different ways.

**Learning from 3D Ground Truth Globally.** Some techniques aim to learn implicit functions that represent conditional mappings from a 3D location to a binary occupancy value [49, 8] or a signed distance value [51, 54]. Early work requires the ground truth occupancy values or signed distance values as 3D supervision. For single image reconstruction, a single image [63, 55, 9, 41, 15, 27] or a learnable latent code [54] can be a condition to provide information about a specified shape. For surface reconstruction [66, 42, 50, 15], we can also leverage a point cloud as a condition to learn an implicit function which can be further leveraged to obtain a mesh surface [35, 12].

**Learning from 3D Ground Truth Locally.** To improve the performance of learning implicit functions, a local strategy was also explored that focuses on more local shape information. Jiang et al. [36] introduced the local implicit grid to improve the scalability and generality. Similarly, Patch-Net [60] was proposed to learn a patch-based surface representation to get more generalizable models. With a grid of independent latent codes, deep local shapes [6] was proposed to represent 3D shapes without prohibitive memory requirements. Using locally interpolated features, convolutional occupancy networks [57] learn occupancy network for 3D scene reconstruction. Other local deep implicit functions [14] are learned by inferring the space decomposition

and local deep implicit function learning from a 3D mesh or posed depth images.

**Learning from 2D Supervision.** We can also learn implicit functions from 2D supervision, such as multiple images. Vincent et al. [56] learned a mapping from world coordinates to a feature representation of local scene properties, which reduces the computational cost on sampling points for implicit surface learning. Inspired by ray marching rendering, differentiable renderers [45, 37, 68] were introduced to render signed distance functions into images. In addition, ray-based field probing [44] or aggregating detection points on rays [67] were employed to mine supervision for 3D occupancy fields. With the implicit differentiation, Niemeyer et al. [53] analytically derived in a differentiable rendering formulation for implicit shape and texture representations. For view synthesis, radiance fields were learned by a neural network first, and then rendered using the naturally differentiable volume rendering to calculate the loss [52].

**Learning from Point Clouds.** Without ground truth signed distance values or occupancy values, learning implicit functions directly from raw point clouds is more challenging. Current methods learn unsigned distance fields with additional constraints, such as geometric regularization [16], sign agnostic learning with a specially designed loss function [1] or constraints on gradients [2], and analytical gradients [10]. A recent concurrent work [10] sharing a similar idea with ours learns unsigned distance fields, which still requires direction to move a query location during the testing stage. While our method directly learns SDFs which can be used to directly predict 3D shapes during testing, especially for applications without knowing point clouds during inference, such as single image reconstruction.

## 3. Method

**Problem Statement.** We employ a neural network to learn SDFs that represent 3D shapes. An SDF  $f$  predicts a signed distance value  $s \in \mathbb{R}$  for a query 3D location  $q = [x, y, z]$ . Optionally, we provide an additional condition  $c$  as input, such that  $f(c, q) = s$ . Given ground truth signed distances as supervision, current methods [51, 54] can employ a neural network to learn  $f$  as a regression problem. Different from these methods, we aim to learn SDF  $f$  in a 3D space directly from 3D point cloud  $P = \{p_j, j \in [1, J]\}$ .

**Overview.** We introduce Neural-Pull as a neural network to learn how to pull a 3D space onto the surface represented by the point cloud  $P$ . Rather than leveraging unsigned distances as previous methods [16, 10, 1, 2], Neural-Pull trains an SDF  $f$  to predict signed distances using the point cloud  $P$  and the gradient within the network itself to represent 3D shapes. Neural-Pull tries to learn to pull a query location  $q_i$  which is randomly sampled around the surface to its nearest neighbor  $t_i$  on the surface, where the query locations form

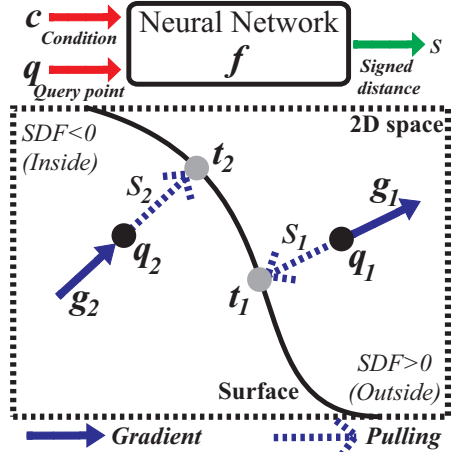


Figure 1. Demonstration of pulling surrounding 2D space to a surface, where gradients  $\mathbf{g}_i$  and signed distance value  $s$  are from neural network  $\mathbf{f}$ .

a set  $\mathbf{Q} = \{q_i, i \in [1, I]\}$ . The pulling operation pulls the query location  $q_i$  with a stride of signed distance  $s_i$ , along or against the direction of the gradient  $\mathbf{g}_i$  at  $q_i$ , obtained within the network.

We demonstrate our idea using a 2D surface in Fig. 1, where the 2D surface splits the space into inside and outside of the shape. We aim to train a neural network to employ the predicted signed distances  $s_1$  (or  $s_2$ ) to pull the query location  $q_1$  (or  $q_2$ ) to its nearest neighbor  $t_1$  (or  $t_2$ ) against (or along) the gradient  $\mathbf{g}_1$  (or  $\mathbf{g}_2$ ) at the query location  $q_1$  (or  $q_2$ ).

**Pulling Query Points.** We pull a 3D query location  $q_i$  to its nearest neighbor  $t_i$  on the surface using the predicted signed distance  $s_i$  and the gradient  $\mathbf{g}_i$  at  $q_i$  within the network. The gradient  $\mathbf{g}_i$  is a vector whose components are the partial derivatives of  $\mathbf{f}$  at  $q_i$ , such that  $\mathbf{g}_i = [\partial \mathbf{f}(\mathbf{c}, \mathbf{q}_i)/\partial x, \partial \mathbf{f}(\mathbf{c}, \mathbf{q}_i)/\partial y, \partial \mathbf{f}(\mathbf{c}, \mathbf{q}_i)/\partial z]$ , which is also denoted as  $\nabla \mathbf{f}(\mathbf{c}, \mathbf{q}_i)$ , where  $\mathbf{c}$  is a condition. It is the direction of the fastest signed distance increase in 3D space. Therefore, we can leverage this property to move a query location along or against the direction of gradient  $\mathbf{g}_i$  to its nearest point on the surface. We leverage the following equation to pull query locations  $q_i$ ,

$$\mathbf{t}'_i = \mathbf{q}_i - \mathbf{f}(\mathbf{c}, \mathbf{q}_i) \times \nabla \mathbf{f}(\mathbf{c}, \mathbf{q}_i) / \|\nabla \mathbf{f}(\mathbf{c}, \mathbf{q}_i)\|_2, \quad (1)$$

where  $\mathbf{t}'_i$  is the pulled query location  $q_i$  after pulling,  $\mathbf{c}$  is the condition to represent ground truth point cloud  $\mathbf{P}$ , and  $\nabla \mathbf{f}(\mathbf{c}, \mathbf{q}_i) / \|\nabla \mathbf{f}(\mathbf{c}, \mathbf{q}_i)\|_2$  is the direction of gradient  $\nabla \mathbf{f}(\mathbf{c}, \mathbf{q}_i)$ . Since  $\mathbf{f}$  is a continuously differentiable function, we can obtain  $\nabla \mathbf{f}(\mathbf{c}, \mathbf{q}_i)$  in the back-propagation process of training  $\mathbf{f}$ . As Fig. 1 demonstrates, for query locations inside of the shape  $\mathbf{P}$ , if the sign of the signed distance value is negative, and the network will move the query loca-

tion  $q_i$  along the direction of gradient to  $\mathbf{t}'_i$  on  $\mathbf{P}$  using  $\mathbf{t}'_i = \mathbf{q}_i + |\mathbf{f}(\mathbf{c}, \mathbf{q}_i)| \times \nabla \mathbf{f}(\mathbf{c}, \mathbf{q}_i) / \|\nabla \mathbf{f}(\mathbf{c}, \mathbf{q}_i)\|_2$ . Instead, the network will move query locations outside of  $\mathbf{P}$  against the direction of gradient due to the positive signed distance value, using  $\mathbf{t}'_i = \mathbf{q}_i - |\mathbf{f}(\mathbf{c}, \mathbf{q}_i)| \times \nabla \mathbf{f}(\mathbf{c}, \mathbf{q}_i) / \|\nabla \mathbf{f}(\mathbf{c}, \mathbf{q}_i)\|_2$ .

**Query Locations Sampling.** We randomly sample query locations around each point  $\mathbf{p}_i$  of the ground truth point cloud  $\mathbf{P}$ . For each point  $\mathbf{p}_i \in \mathbf{P}$ , we establish an isotropic Gaussian function  $\mathcal{N}(\mathbf{p}_i, \sigma^2)$  to form a distribution, according to which we randomly sample 25 query locations, where  $\sigma^2$  is the parameter to control how far away from the surface we can sample query locations. Here, we employ an adaptive way to set  $\sigma^2$  as the square distance between  $\mathbf{p}_i$  and its 50-th nearest neighbor, which reflects location density around  $\mathbf{p}_i$ . The sampled query locations can cover the area around the surface represented by the point cloud  $\mathbf{P}$ , both inside and outside of the shape. Our preliminary results show that sampling near the surface will improve the learning accuracy, since it is hard for the network to predict accurate signed distance and gradient to move a query location that is far from surface to its nearest neighbor on the surface. We will elaborate on the details of leveraging these query locations sampled around  $\mathbf{P}$  during training in the following.

**Loss function.** Neural-pull aims to train a network to learn to pull a query location  $q_i$  to its nearest neighbor  $t_i$  on the point cloud  $\mathbf{P}$ . Therefore, we leverage a mean square error to minimize the distance between the pulled query location  $\mathbf{t}'_i$  obtained in Eq. 1 and the nearest neighbor  $t_i$  of  $\mathbf{p}_i$  on  $\mathbf{P}$  below,

$$d(\{\mathbf{t}'_i\}, \{t_i\}) = \frac{1}{I} \sum_{i \in [1, I]} \|\mathbf{t}'_i - t_i\|_2^2, \quad (2)$$

where  $t_i$  is the nearest neighbor of  $q_i$  on  $\mathbf{P}$ , such that  $t_i = \min_{\mathbf{p} \in \mathbf{P}} \|\mathbf{q}_i - \mathbf{p}\|_2^2$ .

**Training.** We randomly sample  $J = 2 \times 10^4$  points  $\mathbf{p}_j$  from point clouds formed by  $1 \times 10^5$  points released by OccNet [49] as the ground truth point cloud  $\mathbf{P}$  for each shape, where  $j \in [1, J]$ . As mentioned, we sample 25 3D query locations  $q_i$  around each point  $\mathbf{p}_j$  to form the corresponding query location set  $\mathbf{Q}$ , such that  $i \in [1, I]$  and  $I = 5 \times 10^5$ . During training, we randomly select 5000 query locations from  $\mathbf{Q}$  as a batch to train the network. We try two different ways to select the 5000 query locations. One way is to randomly select from  $\mathbf{Q}$ , the other is to uniformly sample 5000 points on the ground truth point cloud  $\mathbf{P}$ , and then select one query location around each sampled point, where the second way can better cover the whole shape in each batch. Our preliminary results show that both of the two ways achieve good learning performance.

We employ a neural network similar to OccNet [49] to learn the signed distance function (more details can be found in our supplemental material). We use the Adam op-

timizer with an initial learning rate of 0.0001, and train the model in 2500 epochs. Moreover, we initialize the parameters in our network using the geometric network initialization (GNI) [1] to approximate the signed distance function of a sphere, where the sign of the signed distance inside of the shape is negative and positive outside.

## 4. Experiments and Analysis

We evaluate our method by comparing it with state-of-the-art methods in surface reconstruction and single image reconstruction.

### 4.1. Surface Reconstruction

**Details.** We employ Neural-Pull to reconstruct 3D surfaces from point clouds. Given a point cloud  $P$ , we do not leverage any condition  $c$  in Fig. 1 and overfit the neural network to the shape by minimizing the loss in Eq. 2, where we remove the network for extracting the feature of the condition. Hence our method does not require any training procedure under the training set, which differentiates our method from the previous ones [1, 10, 42, 12]. After overfitting on each shape, our neural network learns an SDF for the shape. Then, we use the marching cubes [48] algorithm to reconstruct the mesh surface.

**Dataset and Metric.** For fair comparison with other methods, we leverage three widely used benchmarks to evaluate our method in surface reconstruction.

The first benchmark is the ABC dataset [39] which contains a large number and variety of CAD models. We use a subset of this dataset, released by Points2Surf [12] with the same train/test splitting, which contains 4,950 clean watertight meshes for training and 100 meshes for testing.

The second benchmark is FAMOUS which is also released by Points2Surf [12]. The FAMOUS dataset is formed by 22 diverse meshes that are well-known in geometry processing, such as the Utah teapot and the Stanford Bunny.

The third benchmark is a subset of ShapeNet [7], which contains 23,108 CAD models in eight shape classes from ShapeNet. We employ this subset with the same train/test splitting released by MeshingPoint (MeshP) [42].

To comprehensively evaluate our method with the state-of-the-art methods, we leverage different metrics for fair comparison. Following Points2Surf [12], we leverage the L2-Chamfer distance (L2-CD) to evaluate the reconstruction error between our reconstruction and the  $1 \times 10^4$  points ground truth points under the ABC and FAMOUS datasets, where we also randomly sample  $1 \times 10^4$  points on our reconstructed mesh. Besides the L1-Chamfer distance (L1-CD), we also follow MeshP [42] to leverage L2-CD, Normal Consistency (NC) [49], and F-score [59] to evaluate the reconstruction error, where we compare the  $1 \times 10^5$  points sampled on the reconstructed shape with the  $1 \times 10^5$  points sampled on the reconstructed shape with the  $1 \times 10^5$

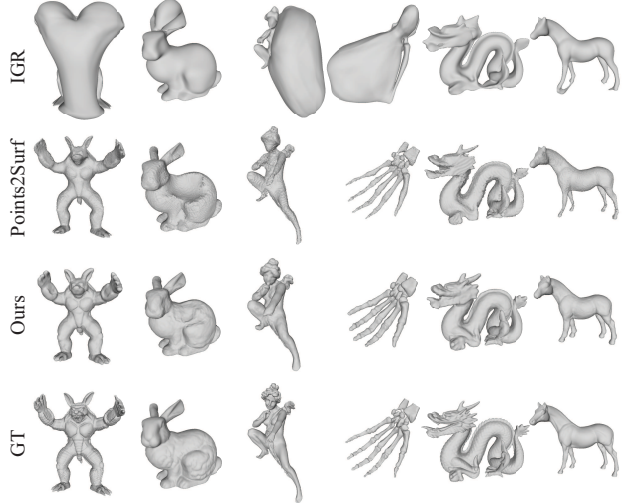


Figure 2. Comparison under FAMOUS in surface reconstruction.

ground truth points released by OccNet [49]. Note that L2-CD leverages the square Euclidean distance as the distance between each pair of points, while L1-CD leverages the Euclidean distance. We also indicate when we multiply by 100 to make the results readable in the caption of the tables.

**Comparison.** We compare our method with state-of-the-art classic and data-driven surface reconstruction methods under the FAMOUS and ABC datasets, including DeepSDF (DSDF) [54], AtlasNet (ATLAS) [17], Screened Poisson Surface Reconstruction (PSR) [38], Points2Surf [12], and IGR [16]. We report the results of DSDF, ATLAS, PSR and Points2Surf from the paper of Points2Surf [12], while reproducing the results of IGR using the official code. The L2-CD comparison in Table 1 shows that our method can significantly increase the surface reconstruction accuracy under each dataset due to better inference of the surface learned in the pulling process.

We visually compare our method with IGR [16] and Points2Surf [12] under the FAMOUS and ABC dataset in Fig. 2 and Fig. 3, respectively. We train IGR using its released code with the same settings as ours, and generate surface reconstruction using the trained parameters released by Points2Surf. The comparison in Fig. 2 demonstrates that our method can reveal geometry details in higher accuracy than other methods. Moreover, the comparison in Fig. 3 shows that our method can reconstruct a smoother plane than Points2Surf, but Points2Surf is good at reconstructing sharp edges.

Similarly, we compare the state-of-the-art classic and data-driven methods under the ShapeNet subset, including PSR [38], Marching Cube (APSS variant) [48], Ball-Pivoting algorithm (BPA) [5], ATLAS [17], Deep Geometric Prior (DGP) [66], Deep Marching Cube (DMC) [40], DeepSDF [54], MeshP [42], Neural Unsigned Distance

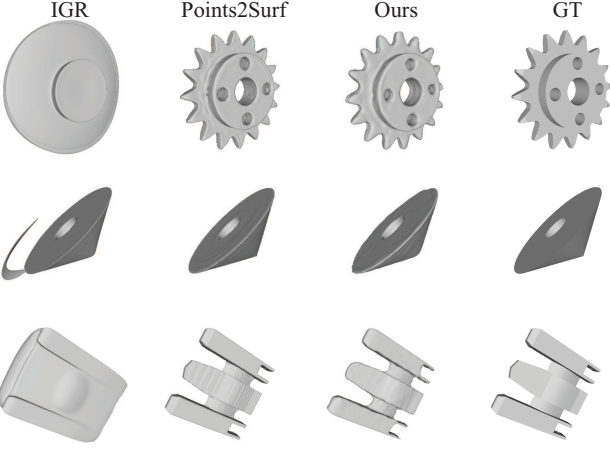


Figure 3. Comparison under ABC in surface reconstruction.

(NUD) [10], SALD [2], Local SDF (GRID) [36], and IMNET [8]. We conduct the numerical comparison in terms of different metrics including L2-CD in Table 2, normal consistency in Table 3, and F-score with a threshold of  $\mu$  in Table 4,  $2\mu$  in Table 5. We report the results of PSR, MC, BPA, ATLAS, DMC, DSDF, DGP, MeshP from the paper of MeshP [42], while reporting the results of SALD, GRID, IMNET from their original papers and reproducing the results of NUD using the same experimental settings. The comparison shown in Table 2, 3, 4, 5 demonstrates that our method can reconstruct more accurate surfaces in terms of CD and F-Score, where we set the threshold  $\mu$  as 0.002 in the F-Score calculation. Although our normal consistency results are comparable to MeshP, MeshP directly does the meshing without learning an implicit function, which requires dense and clean point clouds to guarantee the performance.

We visually compare our method with the-state-of-the-art MeshP [42] under Airplane, Chair, Table and Vessel classes in Fig. 4. We use the parameters trained by MeshP. The comparison shows that our method can reconstruct shapes with more complete surfaces, especially for thin structures or sharp corners, which achieves much higher accuracy.

In addition, we also report our L1-CD results by comparing with 3D-R2 [11], PSGN [13], DMC [40], Occupancy Network (OccNet) [49], and SSRNet [50] under the ShapeNet subset in Table 6. The comparison shows that our method achieves the best performance.

Table 1. Reconstruction comparison in terms of L2-CD ( $\times 100$ ).

Dataset	DSDF	ATLAS	PSR	Points2Surf	IGR	Ours
ABC	8.41	4.69	2.49	1.80	0.51	<b>0.48</b>
FAMOUS	10.08	4.69	1.67	1.41	1.65	<b>0.22</b>
Mean	9.25	4.69	2.08	1.61	1.08	<b>0.35</b>

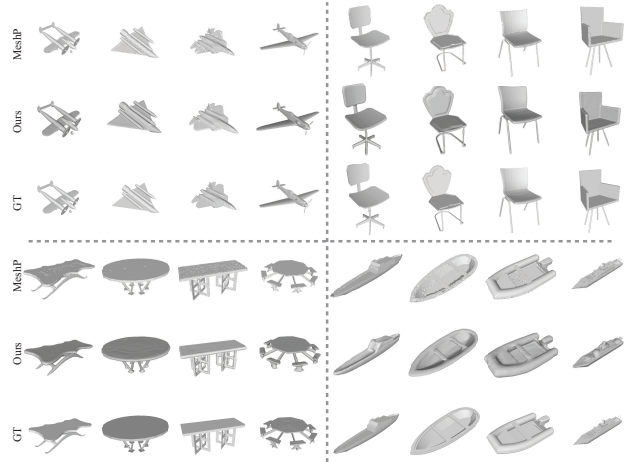


Figure 4. Comparison under ShapeNet in surface reconstruction.

## 4.2. Single Image Reconstruction

**Details.** We further employ Neural-Pull to reconstruct 3D shapes from 2D images. We regard the 2D image as a condition, which corresponds to a 3D shape represented as a point cloud  $P$ . During training, we leverage a condition and a set of query locations  $Q$  to minimize the loss in Eq. 2. During testing, we reconstruct a 3D shape from an input image with a given condition using marching cube [48]. We leverage the 2D encoder used by SoftRas [43] to infer the 2D image conditions.

**Dataset and Metric.** We use the ShapeNet subset released by Choy et al [11] to evaluate the performance in single image reconstruction, where the dataset also contains rendered RGB images in 13 shape classes and a train/test split. After getting the reconstructed meshes, we first leverage the L1-CD and Normal Consistency (NC) to evaluate the reconstruction error between the reconstructed shapes and the  $1 \times 10^5$  ground truth points released by OccNet [49], where we uniformly sample  $1 \times 10^5$  points on the reconstructed shapes. To evaluate our method in a multi-scale way, we also uniformly sample 2048 points on both of reconstructed shapes and  $1 \times 10^5$  point ground truth to evaluate reconstruction error using Earth Mover Distance (EMD).

**Comparison.** We report numerical comparisons with 3D-R2 [11], PSGN [13], Pix2Mesh [61], ATLAS [17], OccNet [49], IMNET [8], 3DN [62], DISN [63] in Table 7. The comparison in terms of L1-CD and Normal Consistency shows that our method can significantly improve the reconstruction performance under almost all shape classes by providing more geometry details on the 3D shapes in higher resolution. The EMD comparison also shows our outperforming results over other methods under a sparse point setting. We further present a visual comparison with ATLAS [17], OccNet [49] and SoftRas [43] in Fig. 5 under Airplane, Chair and Lamp classes, which shows that we

Table 2. Surface reconstruction comparison in terms of L2-CD ( $\times 100$ ).

Class	PSR	DMC	BPA	ATLAS	DMC	DSDF	DGP	MeshP	NUD	SALD	Ours
Display	0.273	0.269	0.093	1.094	0.662	0.317	0.293	0.069	0.077	-	<b>0.039</b>
Lamp	0.227	0.244	0.060	1.988	3.377	0.955	0.167	<b>0.053</b>	0.075	0.071	0.080
Airplane	0.217	0.171	0.059	1.011	2.205	1.043	0.200	0.049	0.076	0.054	<b>0.008</b>
Cabinet	0.363	0.373	0.292	1.661	0.766	0.921	0.237	0.112	0.041	-	<b>0.026</b>
Vessel	0.254	0.228	0.078	0.997	2.487	1.254	0.199	0.061	0.079	-	<b>0.022</b>
Table	0.383	0.375	0.120	1.311	1.128	0.660	0.333	0.076	0.067	0.066	<b>0.060</b>
Chair	0.293	0.283	0.099	1.575	1.047	0.483	0.219	0.071	0.063	0.061	<b>0.054</b>
Sofa	0.276	0.266	0.124	1.307	0.763	0.496	0.174	0.080	0.071	0.058	<b>0.012</b>
Mean	0.286	0.276	0.116	1.368	1.554	0.766	0.228	0.071	0.069	0.062	<b>0.038</b>

Table 3. Surface reconstruction comparison in terms of normal consistency.

Class	PSR	DMC	BPA	ATLAS	DMC	DSDF	MeshP	GRID	IMNET	Ours
Display	0.889	0.842	0.952	0.828	0.882	0.932	<b>0.974</b>	0.926	0.574	0.964
Lamp	0.876	0.872	0.951	0.593	0.725	0.864	<b>0.963</b>	0.882	0.592	0.930
Airplane	0.848	0.835	0.926	0.737	0.716	0.872	<b>0.955</b>	0.817	0.550	0.947
Cabinet	0.880	0.827	0.836	0.682	0.845	0.872	<b>0.957</b>	0.948	0.700	0.930
Vessel	0.861	0.831	0.917	0.671	0.706	0.841	<b>0.953</b>	0.847	0.574	0.941
Table	0.833	0.809	0.919	0.783	0.831	0.901	<b>0.962</b>	0.936	0.702	0.908
Chair	0.850	0.818	0.938	0.638	0.794	0.886	<b>0.962</b>	0.920	0.820	0.937
Sofa	0.892	0.851	0.940	0.633	0.850	0.906	<b>0.971</b>	0.944	0.818	0.951
Mean	0.866	0.836	0.923	0.695	0.794	0.884	<b>0.962</b>	0.903	0.666	0.939

can reconstruct shapes with smoother surface in higher accuracy.

### 4.3. Analysis

**Ablation Study.** We conduct ablation studies in surface reconstruction under FAMOUS dataset. First, we explore the contribution made by the geometric network initialization (GNI). We report the result without GNI as “No GNI” using the random network initialization in Table 8. The degenerated result compared to our method of “Ours” demonstrates that GNI can help the network to better understand the shape. Moreover, we highlight the strategy that we use in the query location sampling near the ground truth point clouds. We replace our sampling by randomly sampling query locations in the entire 3D space, where the number of query locations is kept the same. We report this result as “Space sampling” in Table 8, which demonstrates that it is more effective to use the query locations near the surface to probe the space for the learning. We also try to leverage an additional constraint on the normal of gradient introduced by IGR [16], but the result of “Gradient constraint” shows that the constraints bring no improvement.

**The Effect of Noise.** We further explore the effect of noise on the ground truth point clouds under the ABC and FAMOUS datasets in surface reconstruction. We conduct experiments using the “ABC max-noise” and “FAMOUS max-noise” with strong noise, “ABC var-noise” with varying noise strength, and “FAMOUS med-noise” with a constant noise strength, all of which are released by

Points2Surf [12]. We report our results under these datasets in Table 9, where we show that our method can better resist the noise than the state-of-the-art results. We also visually compare our results with noise and without noise under “FAMOUS med-noise” in Fig. 6. The slight degeneration further demonstrates our ability of learning signed distance functions from point cloud with noise.

**The Effect of Query Location Resolution.** The number of query locations is also a factor that affects the learning. We explore its effect by merely adjusting the number of query locations under FAMOUS in surface reconstruction, such that  $I = \{1, 2.5, 5, 10\} \times 10^6$ . We report the comparison in Table 10, where the best result is achieved with  $I = 10 \times 10^6$ . Moreover, we test the time used in training in one epoch for different numbers of query locations. Although the result with  $I = 10 \times 10^6$  is better than the one with  $I = 5 \times 10^6$  which is used in our previous experiments, it takes much more time in training.

**The Effect of GT Point Cloud Resolution.** We also explore how the resolution of ground truth point clouds affects the performance under the FAMOUS dataset in surface reconstruction in Table 11. We keep the number of query locations the same to  $I = 5 \times 10^6$ , but employ ground truth point clouds with different numbers. Results in Table 11 show that higher resolutions of the ground truth can help our method to better infer the surface, but it also takes much more time to search the nearest neighbor on the ground truth point cloud when calculating the loss, especially in real applications. Moreover, we also compare our method with

Table 4. Surface reconstruction comparison in terms of F-score with a threshold of  $\mu$ .

Class	PSR	DMC	BPA	ATLAS	DMC	DSDF	DGP	MeshP	NUD	GRID	IMNET	Ours
Display	0.468	0.495	0.834	0.071	0.108	0.632	0.417	0.903	0.903	0.551	0.601	<b>0.989</b>
Lamp	0.455	0.518	0.826	0.029	0.047	0.268	0.405	0.855	0.888	0.624	0.836	<b>0.891</b>
Airplane	0.415	0.442	0.788	0.070	0.050	0.350	0.249	0.844	0.872	0.564	0.698	<b>0.996</b>
Cabinet	0.392	0.392	0.553	0.077	0.154	0.573	0.513	0.860	0.950	0.733	0.343	<b>0.980</b>
Vessel	0.415	0.466	0.789	0.058	0.055	0.323	0.387	0.862	0.883	0.467	0.147	<b>0.985</b>
Table	0.233	0.287	0.772	0.080	0.095	0.577	0.307	0.880	0.908	0.844	0.425	<b>0.922</b>
Chair	0.382	0.433	0.802	0.050	0.088	0.447	0.481	0.875	0.913	0.710	0.181	<b>0.954</b>
Sofa	0.499	0.535	0.786	0.058	0.129	0.577	0.638	0.895	0.945	0.822	0.199	<b>0.968</b>
Mean	0.407	0.446	0.769	0.062	0.091	0.468	0.425	0.872	0.908	0.664	0.429	<b>0.961</b>

Table 5. Surface reconstruction comparison in terms of F-score with a threshold of  $2\mu$ .

Class	PSR	DMC	BPA	ATLAS	DMC	DSDF	DGP	MeshP	NUD	Ours
Display	0.666	0.669	0.929	0.179	0.246	0.787	0.607	0.975	0.944	<b>0.991</b>
Lamp	0.648	0.681	0.934	0.077	0.113	0.478	0.662	<b>0.951</b>	0.945	0.924
Airplane	0.619	0.639	0.914	0.179	0.289	0.566	0.515	0.946	0.944	<b>0.997</b>
Cabinet	0.598	0.591	0.706	0.195	0.128	0.694	0.738	0.946	0.980	<b>0.989</b>
Vessel	0.633	0.647	0.906	0.153	0.120	0.509	0.648	0.956	0.945	<b>0.990</b>
Table	0.442	0.462	0.886	0.195	0.221	0.743	0.494	0.963	0.922	<b>0.973</b>
Chair	0.617	0.615	0.913	0.134	0.345	0.665	0.693	0.964	0.954	<b>0.969</b>
Sofa	0.725	0.708	0.895	0.153	0.208	0.734	0.834	0.972	0.968	<b>0.974</b>
Mean	0.618	0.626	0.885	0.158	0.209	0.647	0.649	0.959	0.950	<b>0.976</b>

Table 6. Reconstruction comparison in terms of L1-CD.

3D-R2	PSGN	DMC	OccNet	SSRNet	Ours
0.169	0.202	0.117	0.079	0.024	<b>0.011</b>

DSDF, ATLAS, PSR, Points2Surf under FAMOUS sparser (“F-sparsifier”) and FAMOUS denser (“F-denser”) datasets released by Points2Surf [12]. Results in Table 12 demonstrate that our method also achieves the best results.

**The Effect of Query Locations Range.** Finally, we discuss the effect of the query location range. We use the parameter  $\sigma^2$  to control the maximum range of query locations around each point on the ground truth point cloud. We use several  $\sigma^2$  candidates, including  $\{0.25\sigma^2, 0.5\sigma^2, \sigma^2, 2\sigma^2, 4\sigma^2\}$ , to randomly sample the same number of query locations. We report the results under the FAMOUS dataset in surface reconstruction in Table 13. The comparison shows that a too small or too large query location range will degenerate the surface reconstruction performance. This is because if the query location range is too small, it is hard to use the query locations to probe the area around the surface, while it is also hard to push the network to produce the accurate direction and distance to move the query locations to the surface if the query locations are too far away from the surface.

**Latent Space Visualization.** We visualize the latent space learned by our network in single image reconstruction under ShapeNet subset. We randomly select two reconstructed shapes in the test set of Airplane class or Chair class, and regard their latent codes as two ends to interpolate six new

latent codes between them. We leverage these interpolated latent codes to generate novel shapes by the trained point decoder. We visualize these shape interpolations under each one of Airplane and Chair classes in Fig. 7, which shows that our method can reconstruct complex shapes with arbitrary topology. Moreover, the smooth transformation from one shape to another shape demonstrates that our method can help the network to learn a semantically meaningful latent space.

## 5. Conclusion

We introduce Neural-Pull to learn signed distance functions from 3D point clouds by learning to pull 3D space onto the surface. Without the signed distance value ground truth, we can train a network to learn an SDF by pulling a sampled query location to its nearest neighbor on the surface. We effectively pull query locations along or against the gradient within the network with a stride of the predicted signed distance values. Being able to directly predict signed distances, our method successfully increases the 3D shape representation ability during testing. Our outperforming performance in single image reconstruction and surface reconstruction shows that we can reconstruct shapes and surfaces more accurately and flexibly than the state-of-the-art methods.

## References

- [1] Matan Atzmon and Yaron Lipman. Sal: Sign agnostic learning of shapes from raw data. In *IEEE Conference*

Table 7. Single image reconstruction comparison in terms of different metrics.

	L1-CD, $10^5$ points						Normal Consistency, $10^5$ points						EMD $\times 100,2048$ points					
	3D-R2	PSGN	Pix2Mesh	ATLAS	OccNet	Ours	3D-R2	Pix2Mesh	ATLAS	OccNet	Ours	IMNET	3DN	Pix2Mesh	ATLAS	DISN	Ours	
Airplane	0.227	0.137	0.187	0.104	0.147	<b>0.016</b>	0.629	0.759	0.836	0.840	<b>0.858</b>	2.90	3.30	2.98	3.39	2.67	<b>1.32</b>	
Bench	0.194	0.181	0.201	0.138	0.155	<b>0.016</b>	0.678	0.732	0.779	0.813	<b>0.820</b>	2.80	2.98	2.58	3.22	2.48	<b>1.37</b>	
Cabinet	0.217	0.215	0.196	0.175	0.167	<b>0.018</b>	0.782	0.834	0.850	0.879	<b>0.888</b>	3.14	3.21	3.44	3.36	3.04	<b>1.62</b>	
Car	0.213	0.169	0.180	0.141	0.159	<b>0.022</b>	0.714	0.756	0.836	0.852	<b>0.861</b>	2.73	3.28	3.43	3.72	2.67	<b>1.56</b>	
Chair	0.270	0.247	0.265	0.209	0.228	<b>0.024</b>	0.663	0.746	0.791	<b>0.823</b>	0.810	3.01	4.45	3.52	3.86	2.67	<b>2.03</b>	
Display	0.314	0.284	0.239	0.198	0.278	<b>0.020</b>	0.720	0.830	0.858	0.854	<b>0.867</b>	2.81	3.91	2.92	3.12	2.73	<b>1.64</b>	
Lamp	0.778	0.314	0.308	0.305	0.479	<b>0.021</b>	0.560	0.666	0.694	0.731	<b>0.867</b>	5.85	3.99	5.15	5.29	4.38	<b>2.85</b>	
Loudspeaker	0.318	0.316	0.285	0.245	0.300	<b>0.032</b>	0.711	0.782	0.825	0.832	<b>0.849</b>	3.80	4.47	3.56	3.75	3.47	<b>2.10</b>	
Rifle	0.183	0.134	0.164	0.115	0.141	<b>0.019</b>	0.670	0.718	0.725	0.766	<b>0.811</b>	2.65	2.78	3.04	3.35	2.30	<b>1.41</b>	
Sofa	0.229	0.224	0.212	0.177	0.194	<b>0.019</b>	0.731	0.820	0.840	<b>0.863</b>	0.856	2.71	3.31	2.70	3.14	2.62	<b>1.51</b>	
Table	0.239	0.222	0.218	0.190	0.189	<b>0.025</b>	0.732	0.784	0.832	<b>0.858</b>	0.810	3.39	3.94	3.52	3.98	3.11	<b>1.99</b>	
Telephone	0.195	0.161	0.149	0.128	0.140	<b>0.018</b>	0.817	0.907	0.923	0.935	<b>0.946</b>	2.14	2.70	2.66	3.19	2.06	<b>1.23</b>	
Vessel	0.238	0.188	0.212	0.151	0.218	<b>0.027</b>	0.629	0.699	0.756	0.794	<b>0.827</b>	2.75	3.92	3.94	4.39	2.77	<b>1.71</b>	
Mean	0.278	0.215	0.216	0.175	0.215	<b>0.021</b>	0.695	0.772	0.811	0.834	<b>0.851</b>	3.13	3.56	3.34	3.67	2.84	<b>2.78</b>	

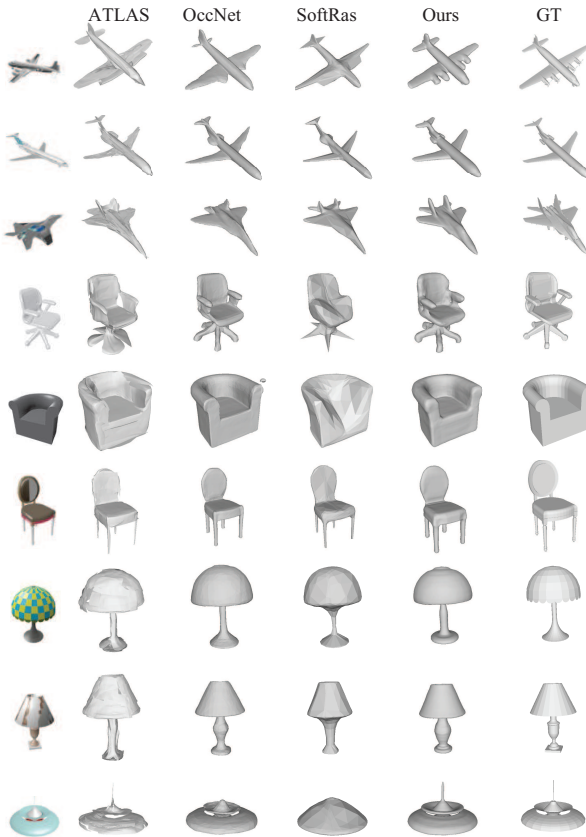


Figure 5. Comparison in single image reconstruction.

Table 8. Ablation studies in terms of L2-CD ( $\times 100$ ).

No GNI	Space sampling	Gradient constraint	Ours
0.35	0.80	1.15	<b>0.22</b>

on Computer Vision and Pattern Recognition, 2020. 1, 2, 4

[2] Matan Atzmon and Yaron Lipman. SALD: Sign agnostic learning with derivatives. *arXiv*, 2006.05400, 2020. 1, 2, 5

[3] Abhishek Badki, Orazio Gallo, Jan Kautz, and

Table 9. Comparison with noise in terms of L2-CD ( $\times 100$ ).

Dataset	DSDF	ATLAS	PSR	Points2Surf	Ours
ABC var-noise	12.51	4.04	3.29	2.14	<b>0.72</b>
ABC max-noise	11.34	4.47	3.89	2.76	<b>1.24</b>
F-med-noise	9.89	4.54	1.80	1.51	<b>0.28</b>
F-max-noise	13.17	4.14	3.41	2.52	<b>0.31</b>
Mean	11.73	4.30	3.10	2.23	<b>0.64</b>

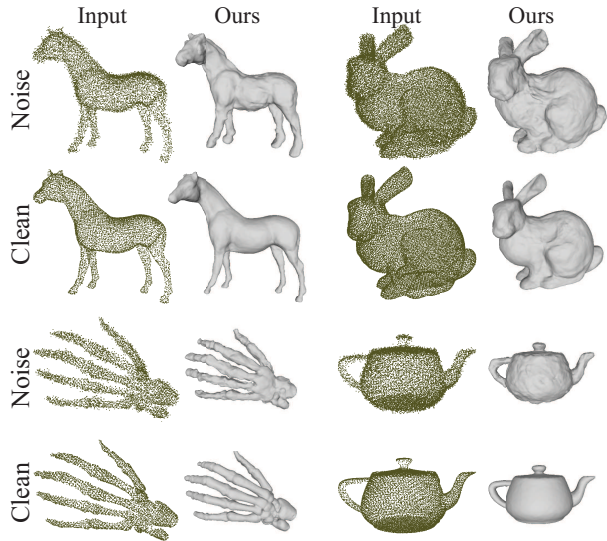


Figure 6. Demonstration of resisting noise.

Table 10. Effect of  $I$  in terms of L2-CD ( $\times 100$ ) and time.

$\times 10^6$	1	2.5	5	10
Accuracy	0.434	0.394	0.223	<b>0.221</b>
Time (s)	103	210	530	1020

Table 11. Effect of  $J$  in terms of L2-CD ( $\times 100$ ).

$\times 10^3$	1	2.5	5	10	20	40
	0.293	0.266	0.236	0.233	0.223	<b>0.213</b>

Pradeep Sen. Meshlet priors for 3D mesh reconstruction. In *IEEE Conference on Computer Vision and Pattern Recognition*, June 2020. 2

[4] Jan Bednarik, Shaifali Parashar, Erhan Gundogdu, and

Table 12. Resolution comparison in terms of L2-CD ( $\times 100$ ).

Dataset	DSDF	ATLAS	PSR	Points2Surf	Ours
F-sparse	10.41	4.91	2.17	1.93	<b>0.84</b>
F-dense	9.49	4.35	1.60	1.33	<b>0.22</b>
Mean	9.60	4.66	1.98	1.62	<b>0.44</b>

Table 13. Effect of  $\sigma^2$  in terms of L2-CD ( $\times 100$ ).

$\times \sigma^2$	0.25	0.5	1	2	4
	0.348	0.304	<b>0.223</b>	0.243	0.271

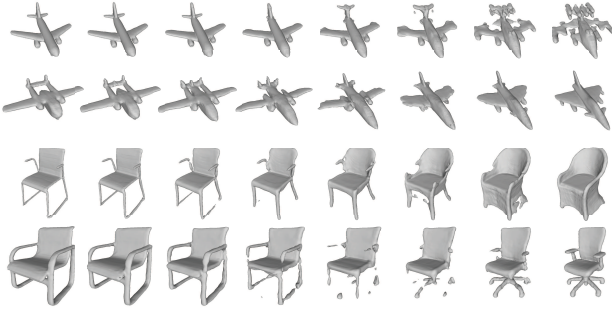


Figure 7. Interpolated shapes in single image reconstruction.

Pascal Salzmann, Mathieu andFua. Shape reconstruction by learning differentiable surface representations. In *CVPR*, 2020. [2](#)

- [5] F. Bernardini, J. Mittleman, H. Rushmeier, C. Silva, and G. Taubin. The ball-pivoting algorithm for surface reconstruction. *IEEE Transactions on Visualization and Computer Graphics*, 5(4):349–359, 1999. [4](#)
- [6] Rohan Chabra, Jan Eric Lenssen, Eddy Ilg, Tanner Schmidt, Julian Straub, Steven Lovegrove, and Richard A. Newcombe. Deep local shapes: Learning local SDF priors for detailed 3D reconstruction. In Andrea Vedaldi, Horst Bischof, Thomas Brox, and Jan-Michael Frahm, editors, *ECCV*, volume 12374, pages 608–625, 2020. [2](#)
- [7] Angel X. Chang, Thomas Funkhouser, Leonidas Guibas, Pat Hanrahan, Qixing Huang, Zimo Li, Silvio Savarese, Manolis Savva, Shuran Song, Hao Su, Jianxiong Xiao, Li Yi, and Fisher Yu. ShapeNet: An Information-Rich 3D Model Repository. Technical Report arXiv:1512.03012 [cs.GR], Stanford University — Princeton University — Toyota Technological Institute at Chicago, 2015. [4](#)
- [8] Zhiqin Chen and Hao Zhang. Learning implicit fields for generative shape modeling. *IEEE Conference on Computer Vision and Pattern Recognition*, 2019. [2, 5](#)
- [9] Julian Chibane, Thimo Alldieck, and Gerard Pons-Moll. Implicit functions in feature space for 3d shape reconstruction and completion. In *IEEE Conference*

*on Computer Vision and Pattern Recognition*, pages 6968–6979, 2020. [2](#)

- [10] Julian Chibane, Aymen Mir, and Gerard Pons-Moll. Neural unsigned distance fields for implicit function learning. *arXiv*, 2010.13938, 2020. [1, 2, 4, 5](#)
- [11] Christopher Bongsoo Choy, Danfei Xu, JunYoung Gwak, Kevin Chen, and Silvio Savarese. 3D-R2N2: A unified approach for single and multi-view 3D object reconstruction. In *Proceedings of European Conference on Computer Vision*, pages 628–644, 2016. [5](#)
- [12] Philipp Erler, Paul Guerrero, Stefan Ohrhallinger, Niloy J. Mitra, and Michael Wimmer. Points2Surf: Learning implicit surfaces from point clouds. In Andrea Vedaldi, Horst Bischof, Thomas Brox, and Jan-Michael Frahm, editors, *ECCV*, 2020. [1, 2, 4, 6, 7](#)
- [13] Haoqiang Fan, Hao Su, and Leonidas J. Guibas. A point set generation network for 3D object reconstruction from a single image. In *IEEE Conference on Computer Vision and Pattern Recognition*, pages 2463–2471, 2017. [5](#)
- [14] Kyle Genova, Forrester Cole, Avneesh Sud, Aaron Sarna, and Thomas Funkhouser. Local deep implicit functions for 3d shape. In *IEEE Conference on Computer Vision and Pattern Recognition*, June 2020. [2](#)
- [15] Kyle Genova, Forrester Cole, Daniel Vlasic, Aaron Sarna, William T. Freeman, and Thomas Funkhouser. Learning shape templates with structured implicit functions. In *International Conference on Computer Vision*, 2019. [2](#)
- [16] Amos Gropp, Lior Yariv, Niv Haim, Matan Atzmon, and Yaron Lipman. Implicit geometric regularization for learning shapes. *arXiv*, 2002.10099, 2020. [1, 2, 4, 6](#)
- [17] Thibault Groueix, Matthew Fisher, Vladimir G. Kim, Bryan C. Russell, and Mathieu Aubry. A papier-mâché approach to learning 3D surface generation. In *IEEE Conference on Computer Vision and Pattern Recognition*, 2018. [2, 4, 5](#)
- [18] Zhizhong Han, Chao Chen, Yu-Shen Liu, and Matthias Zwicker. DRWR: A differentiable renderer without rendering for unsupervised 3D structure learning from silhouette images. In *ICML*, 2020. [2](#)
- [19] Zhizhong Han, Chao Chen, Yu-Shen Liu, and Matthias Zwicker. ShapeCaptioner: Generative caption network for 3D shapes by learning a mapping from parts detected in multiple views to sentences. In *ACM International Conference on Multimedia*, 2020. [2](#)
- [20] Zhizhong Han, Xinhai Liu, Yu-Shen Liu, and Matthias Zwicker. Parts4Feature: Learning 3D global features

from generally semantic parts in multiple views. In *IJCAI*, 2019. 2

[21] Zhizhong Han, Zhenbao Liu, Junwei Han, Chi-Man Vong, Shuhui Bu, and C.L.Philip Chen. Mesh convolutional restricted boltzmann machines for unsupervised learning of features with structure preservation on 3D meshes. *IEEE Transactions on Neural Network and Learning Systems*, 28(10):2268 – 2281, 2017. 2

[22] Zhizhong Han, Zhenbao Liu, Junwei Han, Chi-Man Vong, Shuhui Bu, and C.L.P. Chen. Unsupervised learning of 3D local features from raw voxels based on a novel permutation voxelization strategy. *IEEE Transactions on Cybernetics*, 49(2):481–494, 2019. 2

[23] Zhizhong Han, Zhenbao Liu, Junwei Han, Chi-Man Vong, Shuhui Bu, and Xuelong Li. Unsupervised 3D local feature learning by circle convolutional restricted boltzmann machine. *IEEE Transactions on Image Processing*, 25(11):5331–5344, 2016. 2

[24] Zhizhong Han, Zhenbao Liu, Chi-Man Vong, Yu-Shen Liu, Shuhui Bu, Junwei Han, and C.L.Philip Chen. BoSCC: Bag of spatial context correlations for spatially enhanced 3D shape representation. *IEEE Transactions on Image Processing*, 26(8):3707–3720, 2017. 2

[25] Zhizhong Han, Zhenbao Liu, Chi-Man Vong, Yu-Shen Liu, Shuhui Bu, Junwei Han, and CL Philip Chen. Deep Spatiality: Unsupervised learning of spatially-enhanced global and local 3D features by deep neural network with coupled softmax. *IEEE Transactions on Image Processing*, 27(6):3049–3063, 2018. 2

[26] Zhizhong Han, Honglei Lu, Zhenbao Liu, Chi-Man Vong, Yu-Shen Liu, Matthias Zwicker, Junwei Han, and C.L. Philip Chen. 3D2SeqViews: Aggregating sequential views for 3D global feature learning by cnn with hierarchical attention aggregation. *IEEE Transactions on Image Processing*, 28(8):3986–3999, 2019. 2

[27] Zhizhong Han, Guanhui Qiao, Yu-Shen Liu, and Matthias Zwicker. SeqXY2SeqZ: Structure learning for 3D shapes by sequentially predicting 1D occupancy segments from 2D coordinates. In *ECCV*, 2020. 2

[28] Zhizhong Han, Mingyang Shang, Yu-Shen Liu, and Matthias Zwicker. View Inter-Prediction GAN: Unsupervised representation learning for 3D shapes by learning global shape memories to support local view predictions. In *AAAI*, pages 8376–8384, 2019. 2

[29] Zhizhong Han, Mingyang Shang, Zhenbao Liu, Chi-Man Vong, Yu-Shen Liu, Matthias Zwicker, Junwei Han, and C.L. Philip Chen. SeqViews2SeqLabels: Learning 3D global features via aggregating sequential views by rnn with attention. *IEEE Transactions on Image Processing*, 28(2):685–672, 2019. 2

[30] Zhizhong Han, Mingyang Shang, Xiyang Wang, Yu-Shen Liu, and Matthias Zwicker. Y2Seq2Seq: Cross-modal representation learning for 3D shape and text by joint reconstruction and prediction of view and word sequences. In *AAAI*, pages 126–133, 2019. 2

[31] Zhizhong Han, Xiyang Wang, Yu-Shen Liu, and Matthias Zwicker. Multi-angle point cloud-vae:unsupervised feature learning for 3D point clouds from multiple angles by joint self-reconstruction and half-to-half prediction. In *ICCV*, 2019. 2

[32] Zhizhong Han, Xiyang Wang, Chi-Man Vong, Yu-Shen Liu, Matthias Zwicker, and C.L. Philip Chen. 3DViewGraph: Learning global features for 3D shapes from a graph of unordered views with attention. In *IJCAI*, 2019. 2

[33] Tao Hu, Zhizhong Han, Abhinav Shrivastava, and Matthias Zwicker. Render4Completion: Synthesizing multi-view depth maps for 3D shape completion. *ArXiv*, abs/1904.08366, 2019. 2

[34] Tao Hu, Zhizhong Han, and Matthias Zwicker. 3D shape completion with multi-view consistent inference. In *AAAI*, 2020. 2

[35] Meng Jia and Matthew Kyan. Learning occupancy function from point clouds for surface reconstruction. *arXiv*, 2010.11378, 2020. 1, 2

[36] Chiyu Jiang, Avneesh Sud, Ameesh Makadia, Jingwei Huang, Matthias Nießner, and Thomas Funkhouser. Local implicit grid representations for 3d scenes. In *IEEE Conference on Computer Vision and Pattern Recognition*, 2020. 2, 5

[37] Yue Jiang, Dantong Ji, Zhizhong Han, and Matthias Zwicker. SDFDiff: Differentiable rendering of signed distance fields for 3D shape optimization. In *IEEE Conference on Computer Vision and Pattern Recognition*, 2020. 1, 2

[38] Michael M. Kazhdan and Hugues Hoppe. Screened poisson surface reconstruction. *ACM Trans. Graph.*, 32(3):29:1–29:13, 2013. 4

[39] Sebastian Koch, Albert Matveev, Zhongshi Jiang, Francis Williams, Alexey Artemov, Evgeny Burnaev, Marc Alexa, Denis Zorin, and Daniele Panozzo. Abc: A big cad model dataset for geometric deep learning. In *IEEE Conference on Computer Vision and Pattern Recognition*, June 2019. 4

[40] Yiyi Liao, Simon Donné, and Andreas Geiger. Deep marching cubes: Learning explicit surface representations. In *Conference on Computer Vision and Pattern Recognition*, 2018. 4, 5

[41] Gidi Litwin and Lior Wolf. Deep meta functionals for shape representation. In *IEEE International Conference on Computer Vision*, 2019. 2

[42] Minghua Liu, Xiaoshuai Zhang, and Hao Su. Meshing point clouds with predicted intrinsic-extrinsic ratio guidance. In *European Conference on Computer vision*. 2, 4, 5

[43] Shichen Liu, Tianye Li, Weikai Chen, and Hao Li. Soft rasterizer: A differentiable renderer for image-based 3D reasoning. *The IEEE International Conference on Computer Vision*, 2019. 5

[44] Shichen Liu, Shunsuke Saito, Weikai Chen, and Hao Li. Learning to infer implicit surfaces without 3D supervision. In *Advances in Neural Information Processing Systems*, 2019. 2

[45] Shaohui Liu, Yinda Zhang, Songyou Peng, Boxin Shi, Marc Pollefeys, and Zhaopeng Cui. DIST: Rendering deep implicit signed distance function with differentiable sphere tracing. In *IEEE Conference on Computer Vision and Pattern Recognition*, 2020. 1, 2

[46] Xinhai Liu, Zhizhong Han, Yu-Shen Liu, and Matthias Zwicker. Point2Sequence: Learning the shape representation of 3D point clouds with an attention-based sequence to sequence network. In *AAAI*, pages 8778–8785, 2019. 2

[47] Xinhai Liu, Zhizhong Han, Wen Xin, Yu-Shen Liu, and Matthias Zwicker. L2G auto-encoder: Understanding point clouds by local-to-global reconstruction with hierarchical self-attention. In *ACMMM*, 2019. 2

[48] William E. Lorensen and Harvey E. Cline. Marching cubes: A high resolution 3d surface construction algorithm. *Computer Graphics*, 21(4):163–169, 1987. 4, 5

[49] Lars Mescheder, Michael Oechsle, Michael Niemeyer, Sebastian Nowozin, and Andreas Geiger. Occupancy networks: Learning 3D reconstruction in function space. In *IEEE Conference on Computer Vision and Pattern Recognition*, 2019. 2, 3, 4, 5

[50] Zhenxing Mi, Yiming Luo, and Wenbing Tao. Ssrnet: Scalable 3d surface reconstruction network. In *IEEE Conference on Computer Vision and Pattern Recognition*, June 2020. 2, 5

[51] Mateusz Michalkiewicz, Jhony K. Pontes, Dominic Jack, Mahsa Baktashmotagh, and Anders P. Eriksson. Deep level sets: Implicit surface representations for 3D shape inference. *CoRR*, abs/1901.06802, 2019. 1, 2

[52] Ben Mildenhall, Pratul P. Srinivasan, Matthew Tancik, Jonathan T. Barron, Ravi Ramamoorthi, and Ren Ng. Nerf: Representing scenes as neural radiance fields for view synthesis. In *ECCV*, 2020. 2

[53] Michael Niemeyer, Lars Mescheder, Michael Oechsle, and Andreas Geiger. Differentiable volumetric rendering: Learning implicit 3D representations without 3d supervision. In *IEEE Conference on Computer Vision and Pattern Recognition*, 2020. 2

[54] Jeong Joon Park, Peter Florence, Julian Straub, Richard Newcombe, and Steven Lovegrove. DeepSDF: Learning continuous signed distance functions for shape representation. In *IEEE Conference on Computer Vision and Pattern Recognition*, 2019. 1, 2, 4

[55] Shunsuke Saito, , Zeng Huang, Ryota Natsume, Shigeo Morishima, Angjoo Kanazawa, and Hao Li. PIFu: Pixel-aligned implicit function for high-resolution clothed human digitization. *IEEE International Conference on Computer Vision*, 2019. 1, 2

[56] Vincent Sitzmann, Michael Zollhöfer, and Gordon Wetzstein. Scene representation networks: Continuous 3D-structure-aware neural scene representations. In *Advances in Neural Information Processing Systems*, 2019. 2

[57] Lars Mescheder Marc Pollefeys Andreas Geiger Songyou Peng, Michael Niemeyer. Convolutional occupancy networks. In *European Conference on Computer Vision*, 2020. 2

[58] Matthew Tancik, Pratul P. Srinivasan, Ben Mildenhall, Sara Fridovich-Keil, Nithin Raghavan, Utkarsh Singhal, Ravi Ramamoorthi, Jonathan T. Barron, and Ren Ng. Fourier features let networks learn high frequency functions in low dimensional domains. *NeurIPS*, 2020. 2

[59] Maxim Tatarchenko, Stephan R. Richter, Rene Ranftl, Zhuwen Li, Vladlen Koltun, and Thomas Brox. What do single-view 3D reconstruction networks learn? In *The IEEE Conference on Computer Vision and Pattern Recognition*, 2019. 4

[60] Edgar Tretschk, Ayush Tewari, Vladislav Golyanik, Michael Zollhöfer, Carsten Stoll, and Christian Theobalt. PatchNets: Patch-Based Generalizable Deep Implicit 3D Shape Representations. *ECCV*, 2020. 2

[61] Nanyang Wang, Yinda Zhang, Zhuwen Li, Yanwei Fu, Wei Liu, and Yu-Gang Jiang. Pixel2mesh: Generating 3D mesh models from single RGB images. In *European Conference on Computer Vision*, pages 55–71, 2018. 5

[62] Weiyue Wang, Duygu Ceylan, Radomir Mech, and Ulrich Neumann. 3DN: 3D deformation network. In *CVPR*, 2019. 5

- [63] Weiyue Wang, Qiangeng Xu, Duygu Ceylan, Radomir Mech, and Ulrich Neumann. DISN: Deep implicit surface network for high-quality single-view 3D reconstruction. In *NeurIPS*, 2019. [2](#), [5](#)
- [64] Xin Wen, Zhizhong Han, Geunhyuk Youk, and Yu-Shen Liu. CF-SIS: Semantic-instance segmentation of 3D point clouds by context fusion with self-attention. In *ACM International Conference on Multimedia*, 2020. [2](#)
- [65] Xin Wen, Tianyang Li, Zhizhong Han, and Yu-Shen Liu. Point cloud completion by skip-attention network with hierarchical folding. In *The IEEE Conference on Computer Vision and Pattern Recognition*, 2020. [2](#)
- [66] Francis Williams, Teseo Schneider, Claudio Silva, Denis Zorin, Joan Bruna, and Daniele Panozzo. Deep geometric prior for surface reconstruction. In *IEEE Conference on Computer Vision and Pattern Recognition*, 2019. [2](#), [4](#)
- [67] Yunjie Wu and Zhengxing Sun. DFR: differentiable function rendering for learning 3D generation from images. *Computer Graphics Forum*, 39(5):241–252, 2020. [1](#), [2](#)
- [68] Sergey Zakharov, Wadim Kehl, Arjun Bhargava, and Adrien Gaidon. Autolabeling 3D objects with differentiable rendering of sdf shape priors. In *IEEE Conference on Computer Vision and Pattern Recognition*, 2020. [1](#), [2](#)